Published in ICCS 2009 Proceedings, Eds.: G. Allen, J. Nabrzyski, E. Seidel, D. van Albada,J. Dongarra, and P. Sloot, LNCS 5544, Part I, pp. 695-704. Springer-Verlag, Berlin-Heidelberg, 2009.

Computational upscaling of inertia effects from porescale to mesoscale

Małgorzata Peszyńska[1], Anna Trykozko[2], and Kyle Augustson[3]

[1] Oregon State University, Department of Mathematics,
mpesz@math.oregonstate.edu
[2] Interdisciplinary Centre for Math. and Comp. Modeling, University of Warsaw
aniat@icm.edu.pl,
[3] University of Colorado at Boulder
kyle.augustson@Colorado.edu

Abstract. We propose algorithms for computational upscaling of flow from porescale (microscale) to lab scale (mesoscale). In particular, we solve Navier-Stokes equations in complex pore geometries and average their solutions to derive properties of flow relevant at lab scale such as permeability and inertia coefficients. We discuss two variants of traditional discretizations: a simple algorithm which works well in periodic isotropic media and can be used when coarse approximations are needed, and a more complex one which is well suited for nonisotropic geometries. Convergence of solutions and averaging techniques are major concerns but these can be relaxed if only mesoscopic parameters are needed. The project is a proof-of-concept computational laboratory for porous media which delivers data needed for mesoscale simulations by performing microscale computational simulations.

1 Introduction

Computational modeling of flow in porous media such as aquifers and oil-gas reservoirs has been constrained until recently to the scales of physical observation and of experiments such as Darcy-scale (lab-scale $\equiv$ mesoscale). At the same time, in various applications it has been necessary to *upscale* the models and parameters of flow to macro-scale which is the scale of interest in large porous reservoirs.

In this paper we pursue the upscaling from microscale, i.e., porescale to mesoscale (lab or Darcy scale). While relevant mathematical theory was developed decades ago via homogenization [30] and volume–averaging [25], the computational modeling at porescale, due to its complexity, had remained unfeasible until recently when advances in micro-imaging were accompanied by increases in computational power and development of discrete models such as network and lattice models [26, 22, 19, 29].

In this paper we are interested in continuum models, i.e., traditional discretizations of partial differential equations adapted to porescale such as studies in [1, 13]. We investigate the conditions under which simple algorithms can be

used efficiently to deliver reliable quantitative information from microscale to mesoscale. Our project can be seen as a first step of a computational laboratory for modeling flow over a range of scales; the model at mesoscale can be further upscaled to macroscale by using approach such as one proposed in [7, 14].

The specific following problem is of interest for stationary incompressible viscous flow. It is well known that linear models of flow are not valid beyond certain Reynolds numbers [2], also in porous media [12, 10, 27, 6, 3]. The relevant models are those of Stokes and Navier-Stokes at porescale and Darcy and non-Darcy at mesoscale. Yet identification of a particular regime and of nonlinear models which extend the basic linear models is still a subject of research [20, 25, 17, 21, 16]. While it is now believed that in the nonlinear laminar regime it is the inertia rather than micro-turbulence effects that are most important, no mathematical form of non-Darcy model is yet universally accepted especially in anisotropic media [5, 15, 16], and the values of associated coefficients reported in literature vary significantly [3, 16]. Consider then a scenario in which the experimental data for modeling linear flow at Darcy scale (permeability $\mathbf{K}$) is available but that no data for modeling inertia effects (denoted by β) is given. We propose to i) use the computational porescale model accounting for inertia effects and derive data β for nonlinear models at Darcy scale; here we focus on 2D porescale models with isotropic mesoscale. In addition, one can ii) use these models to investigate anisotropic nonlinear laws at mesoscale that emerge from complicated anisotropic porescale geometries, and aid theoretical developments.

The main difficulties of the project i) are the following. First, even though standard discretization techniques for Navier-Stokes equations are well studied, their use in complex geometries requires fine grids and, in general, is nontrivial. Second, calculating average quantities from computational data is only superficially straightforward since their stability with respect to grids, other computational parameters, and algorithms, over a large range of Reynolds numbers, is necessary. Next, as concerns ii), realistic data on porescale geometries should be used [19], and their uncertainty needs to be accounted for. Finally, computational efficiency of the proposed "on-demand" porescale modeling laboratory must be considered. In this paper we focus on proof-of-concept realization of i); details on ii) will be addressed in a forthcoming paper.

The plan of the paper is as follows. In Section 2 we describe the relevant physical models and in Section 3 the computational models; in Section 4 we propose the method of upscaling. In Section 5 we discuss the computational examples that illustrate the algorithms.

2 Computational models

Let $\Omega \subset \mathbb{R}^d, d = 2, 3$, be an open bounded domain occupied by porous medium and the fluid within. Let $\Omega_F \subsetneq \Omega$ be the part of Ω occupied by the fluid, that is, the domain of flow, and let rock (solid) part be $\Omega_R = \Omega \setminus \Omega_F$. Let $\partial\Omega$ denote the boundary of Ω, and let $\Gamma = \partial\Omega_F \setminus \partial\Omega$ be the interior boundary (between rock and fluid domains) while the external boundary of flow $\partial\Omega_F \cap \partial\Omega$ is divided into

inflow Γ_{in} and outflow Γ_{out} parts. We also denote by η the unit outward normal to the boundary and by τ the unit tangent. For simplicity no special notation is used for numerical solutions.

Flow at porescale. We consider an incompressible Newtonian fluid of velocity $\mathbf{u}$ and pressure p flowing in Ω_F characterized by viscosity μ (fixed). In what follows the fluid's constant density $\rho \equiv 1$. We also assume that the characteristic quantities of the flow are such that the Reynolds number $\mathbf{Re}$ is correlated to the magnitude of inflow velocities.

At microscale (porescale), for steady-state flow, in the absence of forces and mass source/sink terms, the momentum and mass conservation in Eulerian frame are expressed by Navier-Stokes equations and continuity equation [2]

$$\mathbf{u} \cdot \nabla \mathbf{u} - \mu \triangle \mathbf{u} = -\nabla p, \tag{1}$$

$$\nabla \cdot \mathbf{u} = 0. \tag{2}$$

In 2D ($d = 2$) it is convenient to consider the formulation in terms of the vorticity vector $\omega = \nabla \times \mathbf{u}$ and the (scalar) stream function ψ defined by $\mathbf{u} = \nabla \times \psi$ [2]. Taking $\nabla\times$ equation (1) and noticing $\nabla \times (\nabla p) = 0$, one obtains the system

$$\boldsymbol{u} \cdot \nabla \boldsymbol{\omega} = \mu \Delta \boldsymbol{\omega}, \tag{3}$$

$$\Delta \psi = -\omega. \tag{4}$$

The last equation follows from standard calculation $\boldsymbol{\omega} = \nabla \times (\nabla \times \boldsymbol{\psi}) = \nabla(\nabla \cdot \boldsymbol{\psi}) - \Delta \boldsymbol{\psi}$, which, with (2), for 2D flow reduces to (4). We can get p from

$$-\Delta p = (\nabla(\boldsymbol{u} \cdot \nabla)) \cdot \boldsymbol{u} = 2(\frac{\partial u_x}{\partial x}\frac{\partial u_y}{\partial y} - \frac{\partial u_x}{\partial y}\frac{\partial u_y}{\partial x}) \tag{5}$$

For small $\mathbf{Re}$ the nonlinear convective terms associated with $\mathbf{u}\cdot$ are dropped from (1) and (3) and we have the (linear) Stokes approximation

$$-\mu \triangle \mathbf{u} = -\nabla p, \tag{6}$$

which is valid when viscous effects dominate in the flow. For larger $\mathbf{Re}$ the inertia effects associated with $\mathbf{u}\cdot$ cannot be neglected. For even larger $\mathbf{Re}$ in the next regime of flow, the turbulence occurs. We recall that, up to the definition/units of characteristic quantities, the linear laminar flow regime is for $\mathbf{Re} < 1$, the nonlinear regime is for $1 \leq \mathbf{Re} < 100$, and that turbulence may occur for $\mathbf{Re} \geq 100$ [27, 21]; however, turbulence rarely occurs in porous media.

Boundary conditions. We consider flow driven primarily by external boundary conditions which is what would happen experimentally in a lab. We prescribe velocity at the inlet and impose an outflow condition at the outlet. On internal boundaries we assume no-slip condition $\mathbf{u} = 0$.

Flow at Darcy scale. At mesoscale the boundaries between Ω_F and Ω_R are no more recognized, One considers an average pressure $P :=< p >$ and velocity (flux) $\mathbf{U} :=< \mathbf{u} >$ where the averages over a volume $V(\mathbf{x})$ centered at $\mathbf{x} \in \Omega$ are defined as $< q >_V \equiv < q > (x) \equiv \frac{1}{|V(x)|} \int_{V(x)} q(y)dy$. (In what follows we drop subscript V). Conservation of mass after averaging yields $\nabla \cdot < \mathbf{u} >= 0$; note that derivatives in ∇ are taken with respect to large scale variable $\mathbf{x}$.

Darcy's law is a linear momentum equation at mesoscale which can be proven [4, 30] to be an average of Stokes flow (6)

$$\mu \mathbf{K}^{-1} < \mathbf{u} >= -\nabla < p > \tag{7}$$

Here $\mathbf{K}$, a symmetric tensor, is a permeability usually measured in a lab. Due to large viscous dissipation and the interstitial effects typical in porous media, Darcy's law is a good approximation for a large class of flow phenomena. $\mathbf{K}$ reflects geometry at microscale, and $\mathbf{K}^{-1}$ measures resistance of porous medium to the flow. For heterogenous media $\mathbf{K} = \mathbf{K}(\mathbf{x})$, for isotropic media $\mathbf{K} = K\mathbf{I}$.

In the nonlinear laminar regime with significant inertia, averaging (1) yields

$$\mathcal{K}^{-1}(< \mathbf{u} >) < \mathbf{u} >= -\nabla < p > \tag{8}$$

The form of nonlinear map $\mathcal{K}$ has been the subject of theoretical research [15, 5, 17]. The simplest form of such a model in 1D first proposed by Forchheimer [12] was $\mathcal{K}^{-1}(U) := \mu K^{-1} + \beta |U|$, with multidimensional isotropic version [10, 3, 27, 6]

$$\mathcal{K}^{-1}(< \mathbf{u} >) < \mathbf{u} >:= \left(\mathbf{K}^{-1}\mu + \beta | < \mathbf{u} > |\right) < \mathbf{u} >= - < \nabla p > . \tag{9}$$

Now, while values of $\mathbf{K}$ are available for many porous materials [3], the data for coefficient β is not universally available and/or consistent; moreover, the form of $\mathcal{K}$ itself for general anisotropic 2D and 3D media is still a subject of research [20, 13, 16, 21].

Boundary conditions. The flow in Ω at mesoscale is driven by boundary conditions posed on $\partial\Omega$ which are the averages of porescale external boundary conditions.

Mathematical upscaling from micro- to mesoscale. There are essentially two methodologies that apply. The first, with the use of homogenization theory (H) [4, 30], requires periodic geometry but gives elegant theorems on convergence of the averages of microscale quantities to the appropriate mesoscale quantities when the size of periodic cell goes to 0. The second, volume averaging (VA), does not restrict geometry and proposes that the averaged quantities are reasonably stable if the averaging region (REV $\equiv$ Representative Elementary Volume) is large enough [17]; but it may be difficult to quantify what size of REV is sufficient.

3 Computational models for porescale

For flow in Ω_F, we consider two algorithms $\mathcal{H}$ and $\mathcal{VA}$: they are useful in similar contexts as, respectively, mathematical upscaling methods H and VA; each has advantages and disadvantages. For other algorithms see [31, 9].

We illustrate these two algorithms with results along the following scenario. All flow in Ω is from left to right. The pore geometries are idealized: we envision rock grains as very long cylinders so that every cross-section can be approximated by a 2D computational region with Ω_R being a union of solid disks replicated periodically. The ratio of disk diameters to the size of the period denoted by D ranges from 0.6 to 0.9 in this study. See Figures 1 and 3.

Algorithm $\mathcal{H}$. This simple algorithm solves for (ω, ψ) in $d = 2$ and uses simple structured grids over Ω_F and therefore can be easily adapted to interpret data from porescale imaging [19] without significant investment of time in grid generation. It is based on a central finite difference formulation enhanced by treatment of boundary conditions and post-processing, following [18, 28, 8].

The discretization of (3) and (4) yields

$$(\mu\Delta_h - (\boldsymbol{u} \cdot \nabla_h))\,\omega = 0, \tag{10}$$

$$\Delta_h \psi = -\omega. \tag{11}$$

where the numerical Laplacian Δ_h has the usual 5-point stencil, and the advective term is computed using second order central differences. The coupling in the model is resolved by iteration: given ω^n, i) compute ψ^{n+1} from (11), then ii) calculate velocity $\boldsymbol{u}^{n+1}$ from ψ^{n+1}, then iii) solve (10) for $\omega^{n+\frac{1}{2}}$, and finally iv) compute $\omega^{n+1} = \lambda\omega^{n+\frac{1}{2}} + (1-\lambda)\omega^n$ where λ is the relaxation parameter.

In this algorithm steps i) and ii) require that boundary values of ψ and ω are known, respectively. This is the most delicate part of the algorithm and crucial for porescale computations: an idea how to implement inlet, outlet, and no-slip conditions follows; we refer to [28, 8, 9] for details.

For structured rectangular grids over a periodic cell Ω, the boundary Γ is composed of vertical and horizontal segments only, and the external boundary has either vertical or horizontal $\Gamma_{in}, \Gamma_{out}$. Consider vertical Γ_{in}. On inlet boundary, $\mathbf{u} = (u_x, 0)$ is given and hence ψ has to be constant and given as the integral of u_x while vorticity is given from (4). On the vertical portion of the outlet boundary we have $\frac{\partial\omega}{\partial x} = 0$ and $\frac{\partial\psi}{\partial x} = 0$.

In the interior, we have no-slip boundary conditions $\mathbf{u} = 0$; it follows that $\psi \equiv const$. To find useful conditions for ω, we approximate its second derivative as follows. Consider Taylor expansion $\psi(x+\delta x, y) = \psi(x,y) + \delta x\frac{\partial\psi}{\partial x} + \frac{\delta x^2}{2}\frac{\partial^2\psi}{\partial x^2} + O(\delta x^3)$. But $u_y = -\frac{\partial\psi}{\partial x} = 0$ thus $-\omega = \frac{\partial^2\psi}{\partial x^2} = \frac{2(\psi(x+\Delta x,y)-\psi(x,y))}{\delta x^2} + O(\delta x)$. To recover (post-process for) the velocities and pressures, we use central finite differences in the interior of the domain and appropriate one-sided differences at the boundary. The pressure is found from (5).

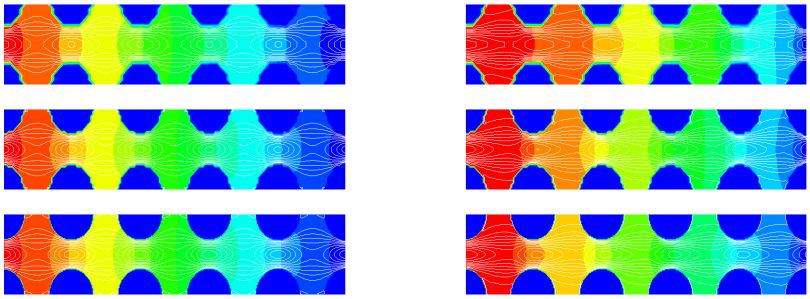

Fig. 1. Results of algorithm $\mathcal{H}$, $D = 0.6$. Shown are profiles of p overlaying contours of $\mathbf{u}$ for $\mathbf{Re} = 1, 100$, (left and right) on three grids: coarse, fine, and very fine (top to bottom). Even though the pointwise values appear unresolved on the coarse meshes, the computed averages and $\mathbf{K}$ and β are stable on all grids

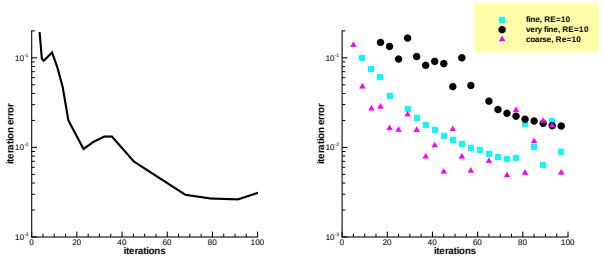

Fig. 2. Algorithm $\mathcal{H}$: convergence of iterative algorithm for standard benchmark problem of Poiseiile flow [9] (left) and for geometry as in Figure 1 (right); the iteration error is defined as discrete l_2 norm of the stream function ψ.

The implementation works well enough for a range of Reynolds numbers and grids that are not very fine, see Figure 1. The difficulties arise since finding an optimal value of λ in step iv) may be a problem; see Figure 2. The simplicity of $\mathcal{H}$ is in that it consequently uses the same Poisson solver for which very efficient solvers e.g. multigrid [9, 31], and preconditioners, are available. An alternative, a coupled solver for (10)–(11) can be written but this requires sophisticated nonsymmetric solvers and preconditioners. Currently $\mathcal{H}$ works well for small periodic domains Ω but may scale poorly to large regions, complex geometries, and large $\mathbf{Re}$

Algorithm $\mathcal{VA}$. This algorithm solves for $(\mathbf{u}, p)$ and can be used in complicated geometries but requires substantial pre-processing; it follows an industry standard in computational fluid dynamics [23, 11]; general unstructured grids can be used in 2D and 3D. We omit the details but provide an example which illustrates the grids and complexity of computations, see Figure 3.

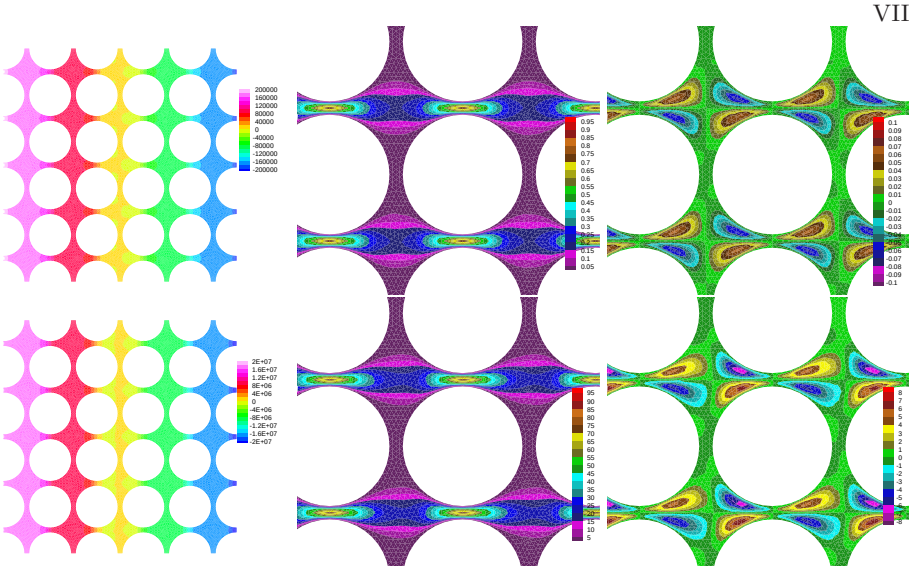

Fig. 3. Results of $\mathcal{VA}$ for $D = 0.9$ with $\mathbf{Re} = 1$ (top) and $\mathbf{Re} = 100$ (bottom). Shown are contours of pressure p (left) and zoomed in velocity $\mathbf{u}$ profiles: component x (middle) and y (right).

4 Upscaling algorithms from porescale to mesoscale

Strictly speaking, the work reported in this paper does not require any computations at mesoscale, i.e., in Ω. However, keeping in mind our future goals, we choose to upscale from microscale to *some chosen* computational grid at mesoscale. In this paper we choose the conservative cell-centered finite difference method equivalent to lowest order Mixed Finite Element method on rectangles [24]; this provides a bridge to macroscale following [14].

The idea is as follows: we impose a mesoscale cell-centered grid over Ω in a way which defines principal directions of flow that we anticipate will prevail at mesoscale (This may help to avoid handling full tensor $\mathbf{K}$ at mesoscale). With each center of mesocale grid (X_j, Y_j), we have an associated cell Ω_j over which we average to get values P_j. Velocities are computed over unions of regions so that they are associated with locations "dual" to those for pressures [24]. Figure 4 illustrates the idea. Ideally, the locations (X_j, Y_j) coincide with centers of mass of Ω_j and the velocity components are computed in the direction of principal axis; but there are ways to handle situations when this does not hold.

Assume now that porescale results $(\mathbf{u}, p)$ are available. We can then compute $\mathbf{U}$ and P as discussed above. Next, by inverse modeling, we can identify resistance of the medium $\mathcal{K}^{-1}$ in discrete counterpart of (8).

Note that for small $\mathbf{Re}$, the resistance $\mathcal{K}^{-1}$ reduces to $\mathbf{K}^{-1}$ as in (7). Thus, if data is available for a large range of $\mathbf{Re}$ from creeping flow to nonlinear laminar regime, then one could hope to identify the appropriate model of tensor $\mathcal{K}$. In particular, if the medium is isotropic at mesoscale, then (9) is valid. In other words, given $\mathcal{K}$ and $\mathbf{K}$ and knowing $\mathbf{U}$, one can compute β for any $\mathbf{Re}$. Clearly

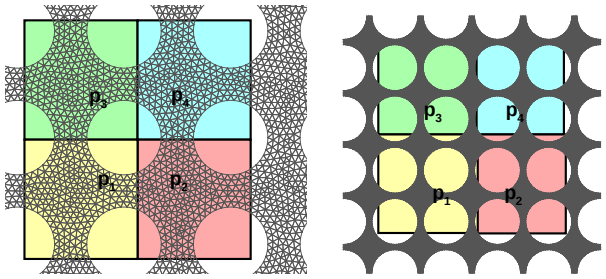

Fig. 4. Left: averaging region for a small periodic region Ω, case $D = 0.7$. The x-component $\mathbf{U}$ can be computed from averaging over regions Ω_1, Ω_3 and Ω_2, Ω_4. Right: general averaging region, case $D = 0.9$.

if the model for $\mathcal{K}$ is valid and the computational algorithm is successful then β remains reasonably constant throughout the nonlinear laminar regime; this appears true in our results, see Figure 5.

We stress that stability of $\mathbf{K}$ and β is not guaranteed with just any ad-hoc averaging technique; in particular, the choice of REV, principal axis and their orientation, and of the boundary conditions, plays a significant role. In addition, there is currently no general explicit mathematical model and virtually no experimental work for anisotropic inertia represented by $\mathcal{K}$. We defer detailed discussion to forthcoming work.

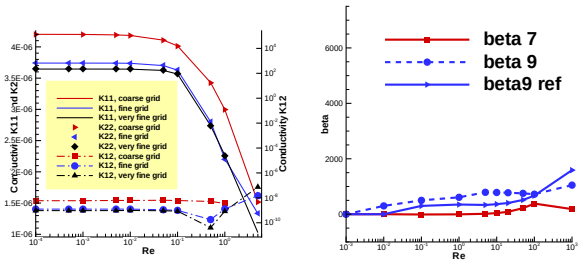

Fig. 5. Results of upscaling from porescale to lab scale. Left: dependence of $\mathbf{K}$ on the grid and $\mathbf{Re}$; notice isotropy at mesoscale revelealed by equal diagonal and very small off-diagonal componets of $\mathcal{K}$. Right: dependence of β on the relative diameter $D \in (0.7, 0.9)$ and on grid size (results computed for coarse and fine grids).

5 Discussion

In this section we revisit and summarize the results presented above and discuss future work.

Fluid flow in porespace is subject to viscous effects, inertia effects, and dissipation on the solid boundaries. In order to approximate it for large $\mathbf{Re}$, we need to ensure that the grid is fine enough in the channels where the solid boundaries

are the closest. Using algorithm $\mathcal{H}$ we could only use $D = 0.6$ while $\mathcal{VA}$ works well for realistic porosities i.e. $D > 0.9$, partly due to unoptimal λ. While we have not found an optimal parameter λ, the convergence of $\mathcal{H}$ appears reasonable for simple cases. Still, more work needs to be done before the algorithm $\mathcal{H}$ can scale to more complicated geometries and large **Re**. In particular, we are considering a transient regularization of (3) which will help the convergence.

The use of algorithm $\mathcal{VA}$, while more promising, also requires care in gridding and monitoring convergence of the iterations. Here the difficulties are related to proper porescale grid definition with respect to principal axis. There is also the relative lack of availability of $\mathcal{VA}$ due to its commercial implementation.

Overall, regardless of the method chosen, for some grids and some **Re**, the profiles of $(\mathbf{u}, p)$ may reveal local instabilities. However, this does not imply instability of mesoscale properties, at least, with the averaging method that we proposed. In fact, **K** and β appear stable for a large range of values of **Re** as well as appear convergent with respect to the grid size, see Figure 5.

Current and future work includes convergence analysis as well as serious computational studies aiding the theoretical modeling of tensor $\mathcal{K}$. Our project is a prototype of a computational laboratory which can provide on-demand model data for flow with inertia in porous media.

Acknowledgements: The work of Peszynska and Augustson was partially supported from NSF grant 0511190 and DOE grant 98089.

References

1. J. S. Andrade, U. M. S. Costa, M. P. Almeida, H. A. Makse, and H. E. Stanley. Inertial effects on fluid flow through disordered porous media. *Phys. Rev. Lett.*, 82(26):5249–5252, Jun 1999.
2. G. K. Batchelor. *An introduction to fluid dynamics*. Cambridge Mathematical Library. Cambridge University Press, Cambridge, paperback edition, 1999.
3. Jacob Bear. *Dynamics of Fluids in Porous Media*. Dover, New York, 1972.
4. Alain Bensoussan, Jacques-Louis Lions, and George Papanicolaou. *Asymptotic analysis for periodic structures*, volume 5 of *Studies in Mathematics and its Applications*. North-Holland Publishing Co., Amsterdam, 1978.
5. Zhangxin Chen, Stephen L. Lyons, and Guan Qin. Derivation of the Forchheimer law via homogenization. *Transp. Porous Media*, 44(2):325–335, 2001.
6. F.L. Dullien. *Porous media*. Academic Press San Diego, 1979.
7. L. J. Durlofsky. Numerical calculation of equivalent grid block permeability tensors for heterogeneous porous media. *Water Resources Research*, 27(5):699–708, 1991.
8. Weinan E and Jian-Guo Liu. Vorticity boundary condition and related issues for finite difference schemes. *J. Comput. Phys.*, 124(2):368–382, 1996.
9. Howard C. Elman, David J. Silvester, and Andrew J. Wathen. *Finite elements and fast iterative solvers: with applications in incompressible fluid dynamics*. Numerical Mathematics and Scientific Computation. Oxford University Press, New York, 2005.
10. S. Ergun. Fluid flow through packed columns. *Chemical Engineering Progress*, 48:89–94, 1952.
11. Fluent Inc. *Fluent User's Guide, ver. 6.3*, 2006.

12. P. Forchheimer. Wasserbewegung durch Boden. *Zeit. Ver. Deut. Ing.*, (45):1781–1788, 1901.
13. M. Fourar, R. Lenormand, M. Karimi-Fard, and R. Horne. Inertia effects in high-rate flow through heterogeneous porous media. *Transport in Porous Media*, 60:353–370(18), September 2005.
14. C.R. Garibotti and M. Peszyńska. Upscaling non-Darcy flow. submitted, 2008.
15. Tiziana Giorgi. Derivation of Forchheimer law via matched asymptotic expansions. *Transport in Porous Media*, 29:191–206, 1997.
16. H. Huang and J. Ayoub. Applicability of the Forchheimer equation for non-Darcy flow in porous media. *SPE Journal*, (SPE 102715):112–122, March 2008.
17. T. Giorgi L. S. Bennethum. Generalized Forchheimer equation for two-phase flow based on hybrid mixture theory. *Transport in Porous Media*, 26(3):261 – 275, March 1997.
18. Rubin H. Landau and Manuel José Páez. *Computational physics*. Wiley, New York, 1997. Problem Solving with Computers.
19. W. Brent Lindquist. Network flow model studies and 3D pore structure. In *Fluid flow and transport in porous media: mathematical and numerical treatment (South Hadley, MA, 2001)*, volume 295 of *Contemp. Math.*, pages 355–366. Amer. Math. Soc., Providence, RI, 2002.
20. C. C. Mei and J.-L. Auriault. The effect of weak inertia on flow through a porous medium. *J. Fluid Mech.*, 222:647–663, 1991.
21. Donald A. Nield and Adrian Bejan. *Convection in porous media*. Springer-Verlag, New York, second edition, 1999.
22. C. Pan, M. Hilpert, and C.T. Miller. Pore-scale modeling of saturated permeabilities in random sphere packings. *Physical Review E.*, 64(066702), 2001.
23. S. V. Patankar. *Numerical Heat Transfer and Fluid Flow FLUENT software*. (Hemisphere, Washington DC, 1980.
24. T. F. Russell and M. F. Wheeler. Finite element and finite difference methods for continuous flows in porous media. In R. E. Ewing, editor, *The Mathematics of Reservoir Simulation*, pages 35–106. SIAM, Philadelphia, 1983.
25. Douglas Ruth and Huiping Ma. On the derivation of the Forchheimer equation by means of the averaging theorem. *Transport in Porous Media*, 7(3):255–264, 1992.
26. M.G. Schaap, M.L. Porter, Christensen B.S.B., and D. Wildenschild. Comparison of pressure-saturation characteristics derived from computed tomography and lattice boltzmann simulations. *Water Resour. Res.*, 43(W12S06), 2007.
27. Adrian E. Scheidegger. *The physics of flow through porous media*. Revised edition. The Macmillan Co., New York, 1960.
28. W. F. Spotz and G. F. Carey. High-order compact scheme for the steady stream-function vorticity equations. *Internat. J. Numer. Methods Engrg.*, 38(20):3497–3512, 1995.
29. Sauro Succi. *The lattice Boltzmann equation for fluid dynamics and beyond*. Numerical Mathematics and Scientific Computation. The Clarendon Press Oxford University Press, New York, 2001. Oxford Science Publications.
30. Luc Tartar. Incompressible fluid flow in a porous medium–convergence of the homogenization process. In *Nonhomogeneous media and vibration theory*, volume 127 of *Lecture Notes in Physics*, pages 368–377. Springer-Verlag, Berlin, 1980.
31. Pieter Wesseling. *Principles of computational fluid dynamics*, volume 29 of *Springer Series in Computational Mathematics*. Springer-Verlag, Berlin, 2001.